CrossMark

Effect of Current Density on Metal Droplet Dropping and Solidification in an ESR System

XIAOHUA WANG [1,3] and YING LI [2]

1.—College of Chemistry, Chemical Engineering and Environmental Engineering, Liaoning Shihua University, Fushun 113001, China. 2.—School of Metallurgy, Northeastern University, Shenyang 110819, China. 3.—e-mail: yuechu1314@foxmail.com

The effects of current density on the multiphase fluid flow and solidification in the electroslag remelting (ESR) system are numerically investigated using the 3D mathematical model. The results show that with the increase of current density, the remelting rate of the consumable electrode increases and the dropping behavior of the molten metal at the electrode tip changes from discontinuous droplets to a continuous stream. Also, the turbulent flow in the slag pool becomes intensive, and both the slag and metal pool temperatures increase, resulting in the formation of a deep U-type metal pool. When the current density increases from 8000 A to 10,000 A, the Joule heat increases from 434.326 kW to 678.635 kW, the remelting rate of the electrode increases from 230 kg/h to 390 kg/h, the maximum temperature in the slag pool increases from 1927 K to 1993 K, and the metal pool depth increases from 115 mm to 182 mm.

INTRODUCTION

The electroslag remelting (ESR) process is an advanced metallurgical technology with functions of secondary refining and directional solidification and is widely used to produce high-quality steels and super alloys with high purity and fine grain.[1–4] During the ESR process, the consumable electrode melts under the effect of Joule heat, and the molten metal drops through the molten slag into the metal pool. The metal droplet formation and falling have a significant impact on the depth and shape of the metal pool and finally affect the solidification direction, composition homogeneity and cleanliness of the ESR ingot. Therefore, knowledge of the metal droplet behavior is of great importance for producing high-quality ingots using ESR technology.

To the authors' knowledge, studies of the metal droplet behavior in the slag pool during the ESR process are relatively few, and most researchers[5–7] take an empirical or semi-empirical formulation to determine the metal droplet shape, distribution and temperature because of the transient two-phase fluid flow and non-isothermal fluid flow problem with magneto-hydrodynamic effects. Giesselmann et al.[8] proposed a novel method that divides the ESR simulation into three different zones to handle different time scales for multiphase flow and thermal equilibrium and adopted a loose coupling scheme to take the interactive effects of melt droplet dropping and magnetohydrodynamics into consideration, where the multiphase fluid flow and heat transfer and the electromagnetic phenomena are respectively solved by using the finite volume method (FVM) and finite element method (FEM). Yu et al.[9] developed a transient two-dimensional (2D) axisymmetry mathematical model to study the effect of the metal droplets on the electromagnetic field, fluid flow and temperature field. Wang et al.[10] developed a transient three-dimensional (3D) finite-volume mathematical model to investigate the coupled physical fields in the ESR process, and the electric potential method, volume of fluid method and enthalpy-porosity method are respectively adopted to solve the electromagnetic field, multiphase fluid flow and solidification at each iteration as a function of the phase distribution. Thus, the fully coupled calculation for the electromagnetic phenomena, multiphase flow and solidification was reached, but the large computation resource and time are still a big challenge for this fully coupled model. Recently, Kharicha et al.[11] developed a 3D magnetohydrodynamic (MHD) model to investigate the complex macroscopic transport phenomena in

the ESR process, such as the electrode smelting, droplet formation and dropping, electromagnetic field, multiphase flow, solidification, etc. It should be mentioned that it is a comprehensive and fully coupled model, which can predict the exact electric and magnetic field distribution in function of the metallic distribution in the slag pool and the interaction between the metal droplet movement and magnetic field in the ESR system. However, this advanced model should be run on a supercomputer and the calculation time is up to about 2 months for the industrial scale ESR process.

Recently, the author[12] has developed a comprehensive 3D mathematical model for simulating multiphase flow and solidification phenomena in an ESR system. Here, the proposed model was adopted to investigate effects of current density on the metal droplet behavior and solidification of ESR ingot.

MODEL DESCRIPTION

Magnetohydrodynamic Model (MHD)

The magnetohydrodynamic phenomena in the ESR system are governed by the following Maxwell equations:[12]

$$\text{Faraday's law: } \nabla \times \mathbf{E} = -\frac{\partial \mathbf{B}}{\partial t} \tag{1}$$

$$\text{Ampere's law: } \nabla \times \mathbf{B} = \mu \mathbf{J} \tag{2}$$

$$\text{Magnetic flux density: } \nabla \cdot \mathbf{B} = 0 \tag{3}$$

$$\text{Ohm's law: } \mathbf{J} = \sigma_c(\mathbf{E} + \mathbf{U} \times \mathbf{B}) \tag{4}$$

Owing to the very low values of the Magnetic Reynolds number, the effect of the metal fluid motion on the Lorentz force field can be neglected by omitting the convection term $\mathbf{U} \times \mathbf{B}$ in Ohm's law.

$$\text{Lorentz force: } F_{em} = \mathbf{J} \times \mathbf{B} \tag{5}$$

$$\text{Joule heat: } Q_J = \mathbf{J} \times \mathbf{E} \tag{6}$$

where $\mathbf{E}$ is the electric field, V/m; $\mathbf{B}$ is the magnetic flux density, T; $\mathbf{J}$ is the current density, A/m^2; $\mathbf{U}$ is the fluid velocity vector, m/s; F_{em} is the Lorentz body force, N/m^3; Q_J is the volumetric Joule power, W/m^3; t is the time, s; μ is the magnetic permeability, H/m; σ_c is the electric conductivity, S/m.

Volume of Fluid Model (VOF)

$$\text{Continuity equation: } \frac{\partial \phi_{st}}{\partial t} + \nabla \cdot (\mathbf{U}\phi_{st}) = 0 \tag{7}$$

$$\text{Momentum equation: } \frac{\partial(\rho\mathbf{U})}{\partial t} + \nabla \cdot (\rho\mathbf{U}\mathbf{U})$$
$$= \nabla \cdot (\bar{\bar{\tau}}) - \nabla \cdot P + F_{em} + F_{vof} + F_{th} \tag{8}$$

$$\bar{\bar{\tau}} = \mu_e\left[\left(\nabla \cdot \mathbf{U} + \nabla \cdot \mathbf{U}^T\right) - \frac{2}{3}\nabla \cdot \mathbf{U}\mathbf{I}\right] \tag{9}$$

where $\mathbf{I}$ is the unit tensor; ϕ_{st} is the local volume fraction of molten steel; P is the static pressure, pa; ρ is the volume-averaged density, kg/m^3; μ_e is the effective viscosity, Pa s; F_{vof} and F_{th} are respectively the volume force induced by the surface tension and the thermal buoyancy force, N/m^3, and can be determined as follows:[13,14]

$$F_{vof} = \sigma_s \frac{\rho\kappa\nabla\phi_{st}}{0.5(\rho_{st} + \rho_{sl})} \tag{10}$$

$$F_{th} = -\rho_0\beta(T - T_0)g \tag{11}$$

where σ_s is the surface tension coefficient, N/m; κ is the curvature of phase interface; ρ_0 is the reference density, kg/m^3; ρ_{st} and ρ_{sl} are respectively the molten steel density and the molten slag density, kg/m^3; T_0 is the reference temperature of the flow, K; T is the temperature of the flow, K; β is the thermal expansion coefficient of the flow; g is the gravitational acceleration, 9.81 m/s^2.

Turbulent Flow Model

Two-equation turbulence models are adopted to describe the turbulent flows in the ESR system in the present study, and the turbulence kinetic energy, k, and the dissipation rate, ε, are obtained as follows:[15]

$$\frac{\partial(\rho k)}{\partial t} + \frac{\partial}{\partial x_i}(\rho u_i k) = \frac{\partial}{\partial x_j}\left[\left(\mu + \frac{\mu_t}{\sigma_k}\right)\frac{\partial k}{\partial x_j}\right] + G_k + G_b - \rho\varepsilon \tag{12}$$

$$\frac{\partial(\rho\varepsilon)}{\partial t} + \frac{\partial}{\partial x_i}(\rho u_i \varepsilon) = \frac{\partial}{\partial x_j}\left[\left(\mu + \frac{\mu_t}{\sigma_\varepsilon}\right)\frac{\partial \varepsilon}{\partial x_j}\right]$$
$$+ C_{1\varepsilon}\frac{\varepsilon}{k}(G_k + C_{3\varepsilon}G_b) - C_{2\varepsilon}\rho\frac{\varepsilon^2}{k} \tag{13}$$

where u_i is a velocity component in x_i direction, m/s; G_k is the generation of turbulence kinetic energy due to the mean velocity gradient; G_b is the generation of turbulence kinetic energy due to the buoyancy; μ and μ_t are respectively the laminar viscosity and the turbulent viscosity ($\rho c_\mu k^2/\varepsilon$), Pa s; $C_{1\varepsilon}$, $C_{2\varepsilon}$, $C_{3\varepsilon}$ and C_μ are constants; σ_k and σ_ε are the turbulent Prandtl numbers for k and ε; the recommended values for $C_{1\varepsilon}$, $C_{2\varepsilon}$, C_μ, σ_k and σ_ε are 1.44, 1.92, 0.09, 1.0 and 1.3, respectively.[15]

Heat Transfer and Solidification Model

The temperature field in the ESR system is governed by the energy conservation equation:

$$\rho \frac{\partial H}{\partial t} + \rho c_p \nabla \cdot (\mathbf{U}T) = \nabla \cdot [(\lambda + \lambda_t) \nabla \cdot T] + Q_J \quad (14)$$

where H is the enthalpy, J/K; C_p is the specific heat, J/(kg K); λ and λ_t are respectively the laminar thermal conductivity and the turbulent thermal conductivity, W/(m K).

Melt Rate Model

The melt rate of the consumable electrode is calculated by using the following heat balance equation at the slag/electrode interface, which was proposed by Choudary and Szekely.[6]

$$m_e [C_{p,e}(T_{l,m} - T_0) + L] = 2\pi \int_0^R r q_{se} dr \quad (15)$$

where m_e is the melt rate, kg/s; $C_{p,e}$ is the specific heat of electrode, J/(kg K); $T_{l,m}$ is the liquidus temperature of steel, K; L is the latent heat, J/kg; R is the electrode radius, m; q_{se} is the heat flux from slag to electrode, W/m².

CALCULATION DESCRIPTION

Materials and Operation Parameters

The consumable electrode material is a rotor steel 30Cr1Mo1V (C: 0.3%, Si: 0.25%, Mn: 0.8%, S: 0.01%, P: 0.01%, Cr: 1.2%, Mo: 1.2%, V: 0.25%), and a classical CaF$_2$-based slag with several oxide additions is used. The main properties required for the simulation are listed in Table I. The ESR is operated with a direct current operation. Here, three cases with different current densities (8000 A, 9000 A and 10,000 A) and the same current frequency of 50 Hz are adopted to investigate the effects of current density on the melt of consumable electrode and solidification during the ESR process.

Calculation Domain

Due to the high temperature and opacity of the ESR system, it is hard to determine the electrode tip shape using the modern detection method on-line, and thus a conical electrode tip is assumed in the present study. Figure 1 shows the schematic diagram of the calculation domain. The radii of the electrode and mold in the ESR are respectively 0.10 m and 0.18 m. The heights of the electrode, slag and ingot are 0.5 m, 0.2 m and 1 m, respectively. The surrounding air region is a cylinder with the radius of 2 m and the height of 2 m and meshed with 3800 volume elements for electromagnetic field calculation. To track the droplet formation and falling in the slag pool during the ESR process, the mesh should be refined at the vicinity of all phase interfaces, especially near the electrode where a thin liquid film develops during the melting process. Therefore, 1.6 million volume elements were meshed in the fluid calculation domain of the slag and a part of ingot with the height of 0.5 m.
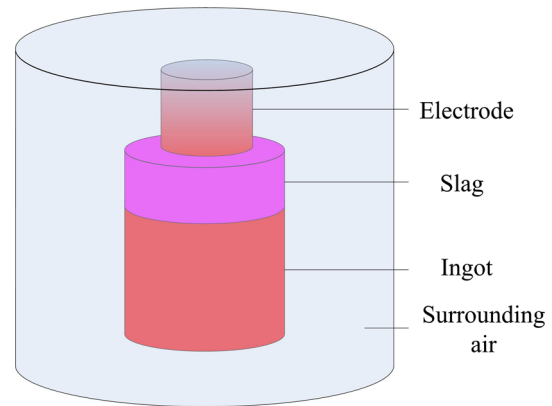

Fig. 1. Schematic illustration of the calculation domain.

Table I. Physical properties of the metal and slag

Properties (units)	Metal	Slag
Electric conductivity (Ω^{-1} m^{-1})	7.14×10^5	175
Magnetic permeability (H m^{-1})	1.26×10^{-6}	1.26×10^{-6}
Density (kg m^{-3})	7.2×10^3	2.85×10^3
Thermal conductivity (W m^{-1} K^{-1})	31.39	10.46
Specific heat (J kg^{-1} K^{-1})	750	1200
Latent heat (J kg^{-1})	2.75×10^5	4.75×10^5
Thermal expansion coefficient (K^{-1})	2.1×10^{-5}	1.0×10^{-4}
Viscosity (kg m^{-1} s^{-1})	6.0×10^{-3}	1.0×10^{-2}
Interfacial tension coefficient (N m^{-1})	0.9	

Table II. The calculated heat generation and melt rate for different current densities

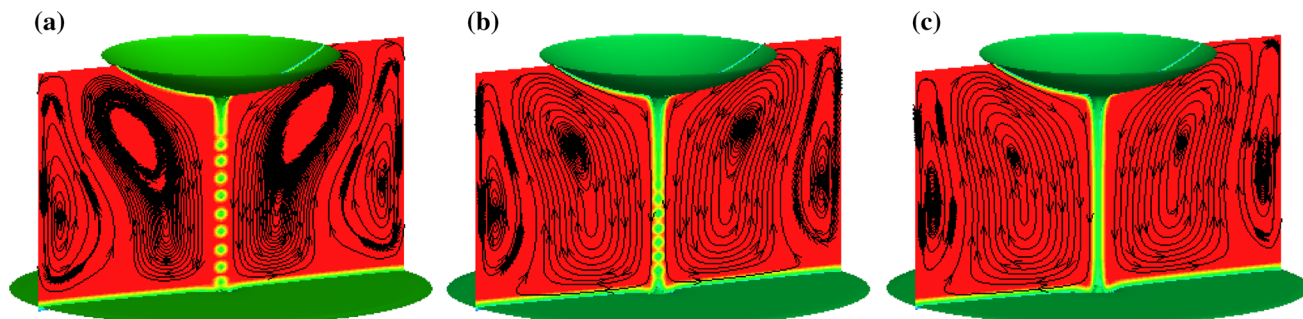|	Current density (A)		
Item	8000	9000	10,000
Joule heat (kW)	434.326	545.003	678.635
Energy for electrode remelting (kW)	79.279	102.497	133.638
Melt rate (kg/h)	230	300	390

Fig. 2. Droplet behavior for different current intensities: (a) 8000 A, (b) 9000 A, (c) 10,000 A.

Boundary Condition

For electromagnetic phenomena, the ESR is operated with the mold electrically connected to the bottom plate. A constant and uniform electric current flow is imposed at the electrode top, and zero electric potential is imposed at the ingot bottom. Because of the electrical insulation of slag skin, no current flow passes through the ingot surface.

For the fluid flow, the inlet and outlet respectively locate at the electrode top and ingot bottom. No-slip conditions are applied at the slag/electrode interface, slag/mold interface and metal/mold interface. A zero shear stress condition is applied at the slag-free surface.

For the heat transfer, the alloy liquidus temperature is applied at the electrode tip. We assume the heat transfer coefficient obeys the linear decrease from top to bottom to simplify the effects of the air gap and slag skin on the heat transfer between the ingot surface and mold.

RESULTS AND DISCUSSION

The calculated heat generation and melt rate for different current densities are listed in Table II. It is obvious that when the current density increases from 8000 A to 10,000 A, the Joule heat increases from 434.326 kW to 678.635 kW, the energy for the electrode remelting provided by slag pool increases from 79.279 kW to 133.638 kW, and the remelting rate of the consumable electrode increases from 230 kg/h to 390 kg/h. That is to say a higher current density results in a higher remelting rate of the

consumable electrode, because higher current density provides more energy for consumable electrode remelting.

Figure 2 shows the metal droplet dropping behavior and streamline of multiphase fluid flow in the slag pool. It can be seen that for the current density of 8000 A, small melt droplets continuously form and depart from the conical electrode tip. With the increase of current density, the remelting rate of the consumable electrode increases and the dropping behavior of the molten metal at the electrode tip changes from discontinuous droplets to a continuous stream during the molten metal falling process in the slag pool when the current density reaches 10,000 A. Meanwhile, the vortexes generated by the dominant effects of the Lorentz force and falling droplets become intensive, but the vortexes generated by the dominant effect of thermal buoyancy become weak, because the Lorentz force increases with the increase of current density.

Figure 3 shows the effect of current density on the fluid flow of the axisymmetric plane in both the slag and metal pool during the ESR process. It is obvious that there are two pairs of vortexes in the slag pool. One pair of vortexes is mainly induced by the Lorentz force and the falling droplets under the electrode tip, and another pair of vortexes is mainly induced by the buoyancy. However, the electromagnetic force in the metal pool is relatively small; thus, there is only one pair of external vortex flows in the metal pool, mainly induced by the thermal buoyancy. With the increase of the current density, the two axisymmetric vortexes induced by the Lorentz force and the falling droplets under the electrode tip
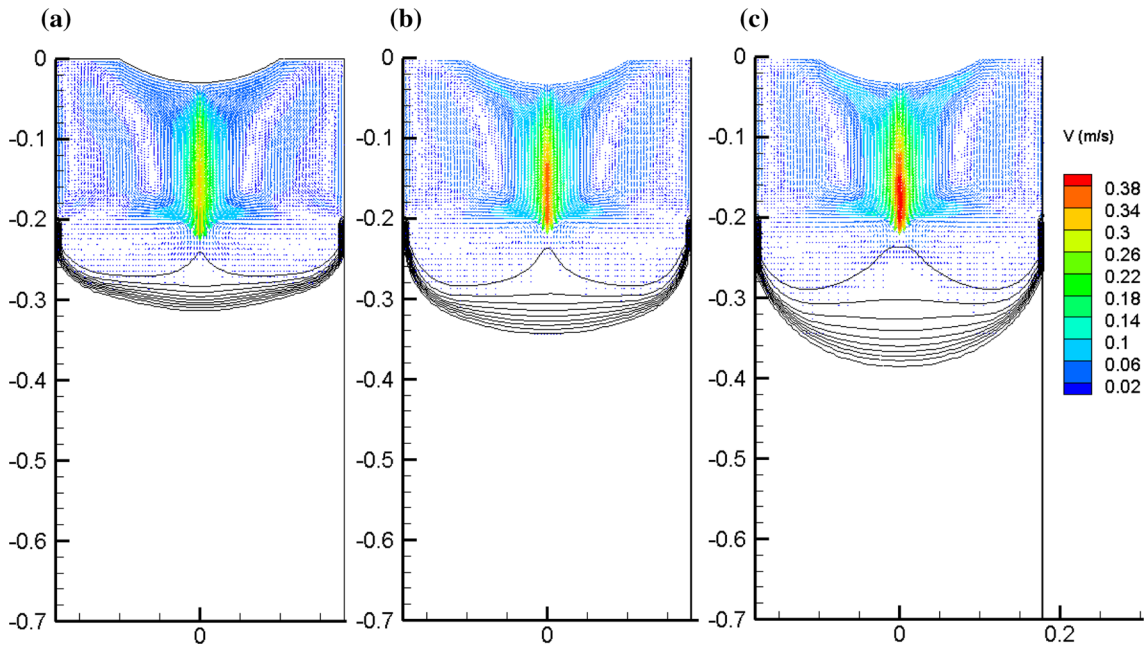
Fig. 3. Velocity field of the main longitudinal section of the ESR system for different current intensities: (a) 8000 A, (b) 9000 A, (c) 10,000 A.
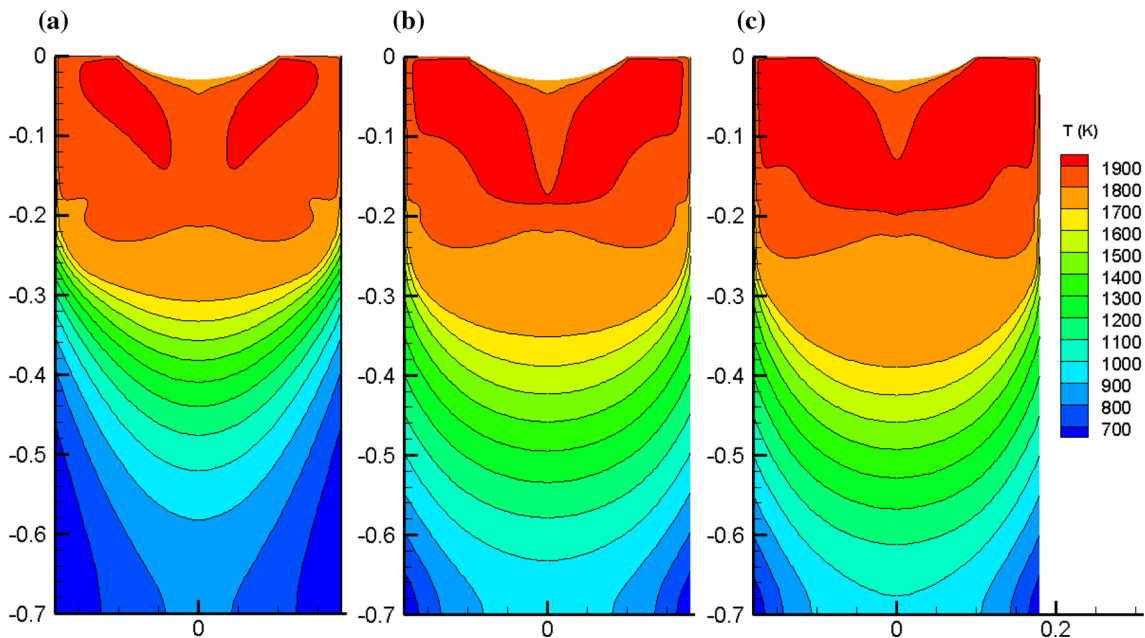

Fig. 4. Temperature field of the main longitudinal section of the ESR system for different current densities: (a) 8000 A, (b) 9000 A, (c) 10,000 A.

become larger and shift downwards because of the increase of the Lorentz force, but the other two axisymmetric vortexes near the mold shift laterally upwards because of the decrease of the Joule heat. Another interesting phenomenon should be mentioned: the maximum velocity of the slag pool increases from 0.35 m/s to 0.40 m/s with the increase of the current density from 8000 A to 10,000 A.

Figure 4 shows the effects of current density on the temperature field in the axisymmetric plane of the ESR system. It can be seen that during the electrode melting process, metal droplet formation and dropping will absorb a large amount of Joule heat from the slag pool, resulting in a low temperature zone formation directly below the electrode in the slag pool. Also, there is a pair of high temperature zones, caused by the vortexes, between the
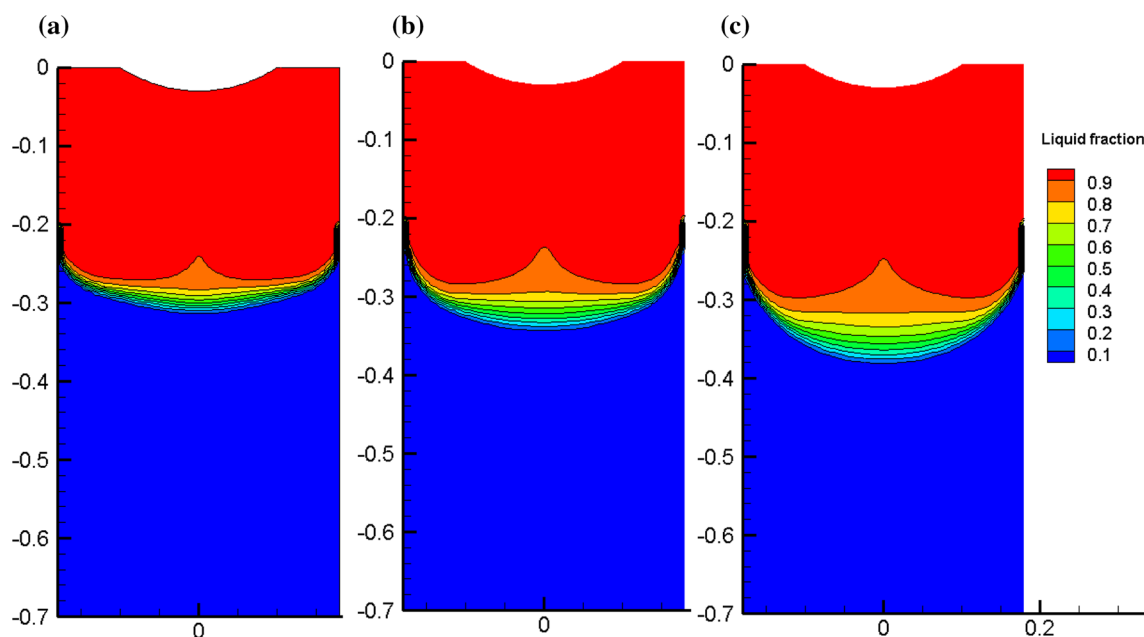
Fig. 5. Liquid pool profile of the ESR system for different current densities: (a) 8000 A, (b) 9000 A, (c) 10,000 A.

electrode and mold laterally. During the dropping process of metal droplets, the metal droplet temperature increases rapidly and finally has the same temperature as the slag pool when the metal droplets left the slag pool. With the increase of current density, the low temperature zone directly below the electrode gradually decreases, but the high temperature zone increases in the slag pool. When the current density increases from 8000 A to 9000 A and 10,000 A, respectively, the maximum temperature in the slag pool increases from 1927 K to 1959 K and 1993 K, respectively. In addition, with the increase of current density, the energy taking from the slag pool into the metal pool by the metal droplets during the dropping process increases, and thus the metal pool temperature increases.

Figure 5 shows the effect of current density on the metal pool profile. It can be seen that the swirling flow has a great influence on the isothermal in the metal pool, especially for the liquidus isotherm. Under the effects of swirling flow in the metal pool, the molten steel with low temperature near the mold lateral flows toward the metal pool center, resulting in the ω-type liquidus isotherm formation. Owing to the bad fluidity in the mushy zone, the swirling flow has little influence on the solidus isothermal and the shape of the molten metal pool is U-shaped. With the increase of current density, the heat transferred from the slag pool to the molten metal pool and the heat carried by the metal droplets dropping through the slag pool increases, resulting in the metal pool temperature and depth increase. Also, with the increase of current density, the effects of current density on the liquidus isotherm become significant and the solidus isotherm gradually moves downwards, resulting in a deep U-type profile. When the current density increases from 8000 A to 9000 A and 10,000 A, respectively, the depth of the metal pool increases from 115 mm to 144 mm and 182 mm, respectively.

CONCLUSION

1. With the increase of current density, the remelting rate of consumable electrode increases and the dropping behavior of the molten metal at the electrode tip changes from the discontinuous droplets to a continuous stream. Also, the turbulent flow in the slag pool becomes intensive, and both the slag and metal pool temperatures increase, resulting in the formation of a deep U-type metal pool.
2. With the increase of current density from 8000 A to 10,000 A, the Joule heat increases from 434.326 kW to 678.635 kW, the remelting rate of the electrode increases from 230 kg/h to 390 kg/h, the maximum temperature in the slag pool increases from 1927 K to 1993 K, and the metal pool depth increases from 115 mm to 182 mm.

ACKNOWLEDGEMENTS

REFERENCES

1. B. Hernandez-Morales and A. Mitchell, *Ironmak. Steelmak.* 26, 423 (1999).
2. A. Mitchell, *Mater. Sci. Eng. A* 413–414, 10 (2005).

3. Y.M. Ferng, C.C. Chieng, and C. Pan, *Numer. Heat Trans. A* 16, 429 (1989).
4. V. Weber, A. Jardy, B. Dussoubs, D. Ablitzer, S. Rybéron, V. Schmitt, S. Hans, and H. Poisson, *Metall. Mater. Trans. B* 40, 271 (2009).
5. A.H. Dilawari and J. Szekely, *Metall. Trans. B* 9, 77 (1978).
6. M. Choudhary and J. Szekely, *Metall. Trans. B* 11, 439 (1980).
7. M. Choudhary, J. Szekely, B.I. Medovar, and Y.G. Emelyanenko, *Metall. Trans. B* 13, 35 (1982).
8. N. Giesselmann, A. Rückert, M. Eickhoff, H. Pfeifer, J. Tewes, and J. Klöwer, *ISIJ Int.* 55, 1408 (2015).
9. J. Yu, Z.H. Jiang, F.B. Liu, K. Chen, H.B. Li, and X. Geng, *ISIJ Int.* 57, 1205 (2017).
10. Q. Wang, Z. He, B.K. Li, and F. Tsukihashi, *Metall. Mater. Trans. B* 45, 2425 (2014).
11. A. Kharicha, A. Ludwing, M. Wu, and E. Karimi-Sibak, *Metall. Mater. Trans. B* 47, 1427 (2016).
12. X.H. Wang and Y. Li, *Metall. Mater. Trans. B* 46, 1837 (2015).
13. J.U. Brackbill, D.B. Kothe, and C. Zemach, *J. Comput. Phys.* 100, 335 (1992).
14. M.G. Worster, *Annu. Rev. Fluid Mech.* 29, 91 (1997).
15. B.E. Launder and D.B. Spalding, *Comput. Methods Appl. Mech. Eng.* 3, 269 (1974).